RSC Advances

ROYAL SOCIETY OF CHEMISTRY

www.rsc.org/advances

RCS Advances

COMMUNICATION

Nanomechanics of Suspended Fibroblast by Point-like Anchors Reveals Cytoskeleton Formation

Sabato Fusco*[,a], Pasquale Memmolo[a,b], Lisa Miccio[b], Francesco Merola[b], Martina Mugnano[b], Antonio Paciello[a], Pietro Ferraro[b] and Paolo A. Netti[a,c]

In an attempt to better elucidate the material-cytoskeleton crosstalk during the initial stage of cell adhesion, here we report how suspended cells anchored to point-like bonds are able to assemble their cytoskeleton when subjected to mechanical stress. The combination of holographic optical tweezers and digital holography gives cells footholds for the adhesion and mechanical stimulation and, at the same time, acts as a label-free, force-revealing system over time, detecting the cell nanomechanical response in the pN range. To confirm the formation of cytoskeleton structures after the stimulation, a fluorescence image system was added as a control. The strategy here proposed portends broad applicability to investigate the correlation between the forces applied to the cells and their cytoskeleton assembly process in this or other complex configurations with multiple anchor points.

Investigating the mechanical crosstalk between the cells and their surrounding environment is fundamental to understand the influence of forces on cell functions and responses[1, 2]. Indeed, the correlation between cells and forces (sensed and generated by cell) has been receiving an increasing interest in biological and biomedical research. In particular, the ability of cells to sense forces is strictly correlated to cytoskeleton dynamics[3-5]. Generally, force transmission is accomplished *via* focal adhesions (FAs)[6]. Cells anchor onto the extracellular substrate through trans-membrane proteins, i.e. integrins, which form bonds with various extracellular protein-receptors, e.g. the adhesive signal Arg-Gly-Asp (RGD). Depending on the magnitude and the distribution of the transmitted forces, cells trigger different cascade pathways of biochemical signals that regulate short and long-term cellular responses and behaviors[7]. Noteworthy, a quantitative determination of the transmitted forces would significantly contribute to shed light on this mechanism, known as mechanotransduction. Until now, the correlation between forces and cell mechanotransduction has been carried out through techniques like traction force microscopy or by using flexible polydimethylsiloxane pillars[8, 9]. Such techniques have helped to understand the nature of the forces exerted by cells on the extracellular surroundings and to quantitatively measure them. This kind of experimental campaigns has been conducted on adherent cells averaging the generated forces on the contact points (FAs) with substrates[10, 11].

To mechanically manipulate suspended cells (i.e. stretching), some optical techniques have been developed. Among these, Optical Tweezers (OT) allow manipulating cells directly in suspension in a contact-less and non-invasive manner[12-16]. OT has been widely exploited for studying cells in a suspended state, such as red blood cells, where the great elasticity of their membranes permits easy deformability, stretching and rotation[17-20]. In particular, Guck and coworkers created a microfluidic cell stretcher able to measure the deformability of membranes of suspended cells by using two counter-propagating laser beams inside a microfluidic channel[21]. The apparatus was able to trap the cells under test and to induce a deformation on the whole cell population. The ability of their apparatus to discern between healthy and cancer cells as a consequence of the different deformability was proofed. Schmidt and coworkers proposed for the first time a dual trap system able to promote cell adhesion in a suspended configuration[22, 23]. The experiments demonstrated that the mechanical responses of the acto-myosin cortical network are responsible for equilibrating cell internal osmotic pressure and shape fluctuations.

In this context, the aim of this paper is to investigate the correlation between force generation and the assembly of cytoskeleton when cells are exposed to mechanical stimulation and anchored only to point-like and predetermined bonds, thus decoupling the influence of the substrates. To this end, we used the capabilities of Holographic OT (HOT) to enable the generation and the independent high-precise control of an

arbitrary number of 3D optical traps. HOT have already been used for mechano-biophysical analysis of the inner structure of living cells[24, 25], cell identification, manipulation and tracking[14, 26-34]. In this work, to analyze and characterize the force dynamics and the cytoskeleton assembly/disassembly in these point-like adherent conditions, we combined the HOT arrangement with two imaging systems, i.e. Digital Holography (DH)[35-39] and fluorescence microscopy. The combination of HOT and DH has been already exploited to study the propagation of the strain inside adherent cells induced by locally applied forces[40]. Here, the system was used to manipulate micrometer latex beads, to anchor them to suspended cells in a predefined configuration and to induce mechanical stimuli and -thus- cell deformation. In particular, the case presented in this work as a proof of concept is the simplest configuration of a single cell suspended between two rigid beads. The corresponding static deformation induced by a single stretching stimulus, kept constant in time, was investigated using a holographic particle tracking approach[27]. The cell mechanical response is discussed in terms of mechanical contributions of cortical and cytoskeletal actin structures. DH imaging measured forces generated in a quantitative, label free and non-invasive way. Furthermore, by DH imaging, an increase of refractive index in the inner volume of the cell was revealed, along the direction connecting the two anchoring points on the beads, as discussed and shown below. We believe that such detected increase in the quantitative phase imaging is due to the assembling of cytoskeletal actin structure. In fact, fluorescence imaging allowed us to confirm the presence and reorganization of such inner structures, as clearly revealed by the experimental results presented in the following.

The optical setup is depicted in **Figure 1a**. A mixture of RGD functionalized beads and cells (NIH/3T3 murine fibroblast) was introduced in a temperature and CO_2 controlled chamber (petri-dish) with optimized concentrations to perform the experiments. The petri-dish was opportunely pre-treated to avoid cell adhesion. First, beads were trapped by HOT (**Figure 1b**) and then moved in contact with the cells (**Figure 1c**) to promote attachment. Digital holograms were numerically processed to simultaneously track the trapped microspheres and recover the Quantitative Phase-Contrast Map (QPM) of the entire field of view in order to monitor the Optical Path Difference (OPD) induced on the cell by the mechanical stresses.

The analysis consisted of the following steps: i) characterization of trapped bead motion in time, by a previously proposed method[27], to detect statistical changes in bead movements before and after static deformation of the cell; ii) QPM reconstructions for cell monitoring to detect shape changes; iii) fluorescence imaging to correlate bead motion and cell shape modifications to cytoskeleton assembly. The main steps of the experiment, which lasted about 1 h, are sketched in **Figures 2 and 3**. Specifically, **Figure 2a** shows two optically trapped microbeads; we reported the displacements in the first 5 min after trapping (3000 points, blue dots of
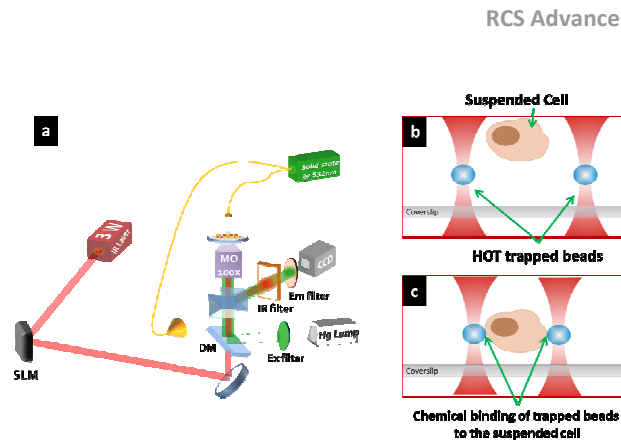
Figure 1. (a) Experimental setup made of HOT, DH and fluorescence moduli. Design of the experiment: one or more beads are optically trapped (b) and attached to a single floating fibroblast (c).

Figure 2e). Similarly, the displacement trend immediately after particle approach and during the attaching phase to the cell membrane is shown in **Figure 2b-f.** The statistical behavior of displacements reported in **Figure 2e** and **Figure 2f** is very similar; however, an average damping of 3% is calculated in the case of attached beads. Nonetheless, we find that this perturbation is completely recovered in the first 5 min after bead attachment. At this time point (20th min), mechanical stretching was imposed on the right side bead shifting it 2 μm along the x-axis. Then, by monitoring the beads after stretching for 10 min (**Figure 2c-g**), no damping of their displacements was observed with respect to the case reported in **Figure 2f**. After this time interval, the tracking measurements revealed that the effect of static stress was a damping in the right bead displacements (**Figure 2d-h**). Because no other stimuli occurred during the experiment, the cell reacted stiffening itself to a static tensional state, as shown by the envelope in the bead displacements. This was confirmed by calculating the trap stiffness (k_{trap}) from bead displacement, over time (see **Figure 3a,b**). Since we calculated an accuracy of 27 nm in the displacement measurements, the corresponding stiffness precision is 0.16 pN/ μm. We found that, before the beads adhere to the cell, trap stiffnesses were 2.7 pN/μm and 2.1 pN/μm along the x and y-axis, respectively, i.e. trapped bead displacements in this first stage presented a typical Brownian behavior. We observed that the stiffness along the x-axis did not change after the attachment to the cell membrane. If we assume that in the system bead-cell-bead the composed elastic constant of trapped beads was $k=k_{trap}+k_{mem}$, where k_{mem} is the membrane stiffness, soon after attachment, total stiffness returned to be approximable to the value before cell-bead engagements ($k=k_{trap}+k_{mem}\approx k_{trap}$). However, a variation of trap stiffness was calculated along the y-axis, allowing a 6% increase of the total stiffness. In addition, we evaluated the exerted force on the cell, which was found to be about 5 pN. Surprisingly, considering the amount of deformation on RBC previously reported[12, 19, 41], the

COMMUNICATION
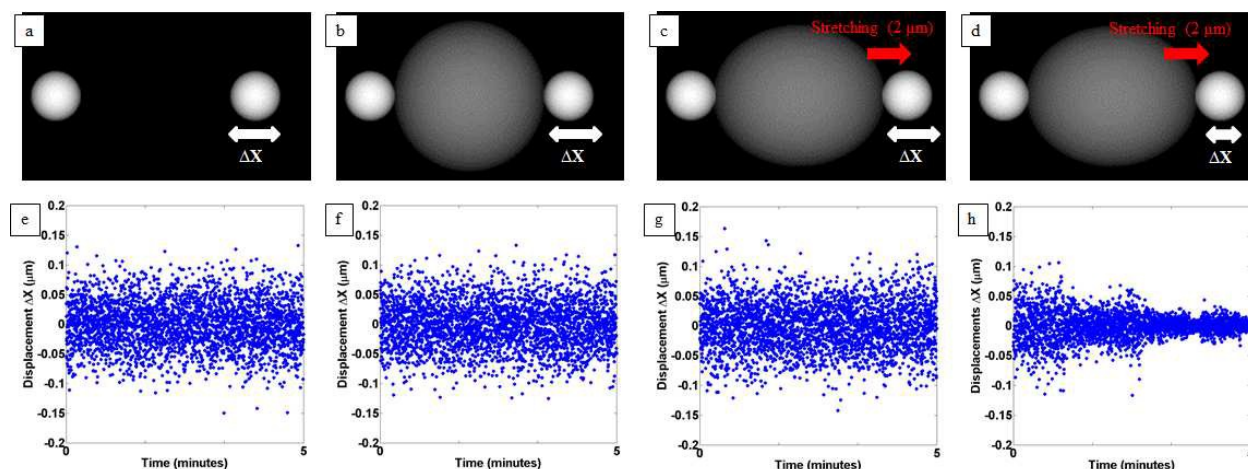
Figure 2. Time evolution windows (5 min) of the bead displacements (blue points) along x-axis before and after stretching (held for the rest of the experiment) by shifting the right bead by 2 μm; (a) when the beads are trapped by HOT they present the classical Brownian motion of a particle in a potential well (e), the same happens immediately after attaching the beads to the cell (b-f). Once stretched, the bead still presents the classical Brownian motion of a particle in a potential well (c-g). Conversely, after 10 min from stretching (d-h) the amplitude of the displacements is considerably reduced.

application of forces with the same order of magnitude (tens of pN) on suspended fibroblast did not produce any detectable deformation, as already observed[23]. This led to the consideration that different mechanical properties and different values of membrane tension were involved. However, around the 30th minute (see **Figure 3a**), trap stiffness started to increase reaching values about 40% and 25% higher than at the beginning, for the right and left beads, respectively. Noteworthy, the trap elastic constants reported in **Figure 3a** were the result of the numerical envelope of the data collected during the experiment. Notice that also a stiffness variation was observed along the *y*-axis, equal to 9% and 13%, for the right and left beads, respectively, as shown in **Figure 3b**. As a consequence, such results produced a correlated displacement between beads, evaluated during the experiment and reported in **Figure 3d**. Interestingly, the mutual correlation factors followed the same trend of the trap stiffness over time. In fact, in the time interval before and after bead attachment, their motions were completely uncorrelated, the correlation factor ranging between 0 and 0.05. After mechanical stimulation, the correlation factor increased to ~ 0.2, thus indicating that the bead oscillation around the trap equilibrium position began decreasing. No correlation was observed orthogonally to the stretching.

The previous evaluation was devoted to understand the temporal evolution of cell behavior through its stiffness and the correlation between trapped beads. However, in order to calculate the instantaneous forces exerted by the fibroblasts we considered independently the different intervals of time reported in **Figure 2** and the corresponding displacement measurements. This analysis furnished a different stiffness

value with respect to that of **Figure 3a and 3b,** because no temporal correlation was considered. In particular, we calculated an increment of the absolute elastic constant from 2.6 to 29.4 pN/μm for the right bead along the stretching direction (see **Table S1**). Another interesting effect is reported in **Figure 3c**, where the drift displacements of beads are reported. Both microspheres show a displacement of ~ 0.5 μm (left bead) and ~ 1 μm (right bead) towards the cell nucleus, indicating a cell contraction after mechanical stimulation.
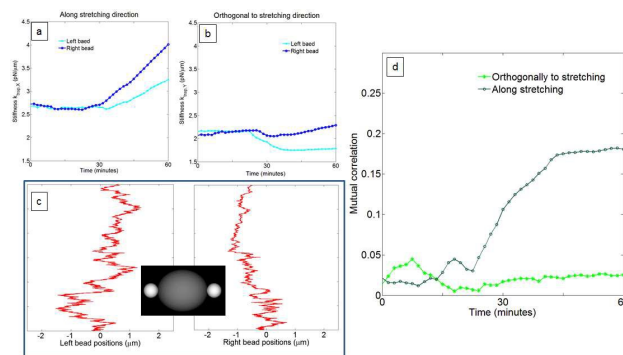
Figure 3 Trap elastic constant measured as a function of time for both beads along *x*-axis (a) and *y*-axis (b), where *x* is the stretching direction. (c) Drift displacements of left and right beads, respectively, demonstrate a cell contraction after mechanical stimulation. In (d) the mutual correlations between left and right displacements in both along *x* and *y*-axis are reported.
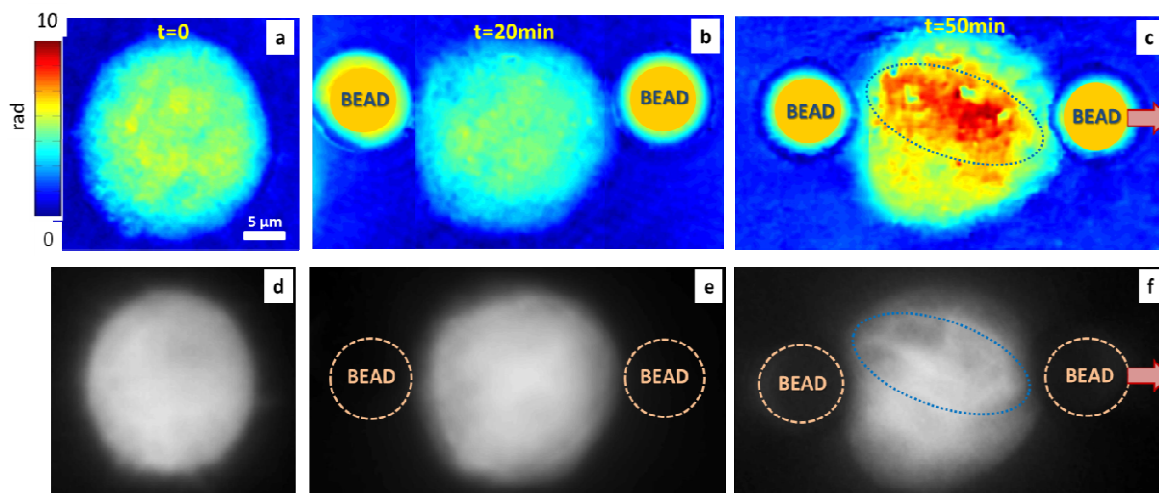
Figure 4 (a,d) are QPM and fluorescent images of a LifeAct-RFP transfected cell in suspension before microbead approaching (t=0) and (b,e) clamped between two microbeads (t=20 min). (c,f) QPM and fluorescence image at t=50 min of the experiment (30 min after stretching), showing the presence of actin aggregates. (c) QPM of the cell shows an enhancement of the OPD signal in correspondence of the area connecting the two microspheres (the dotted line is just a guide for the eye), confirmed by the fluorescence image (f) of the assembling cytoskeleton.

Furthermore, combining such displacement values with the elastic constants of both traps along the stretching axis (8.1 and 29.4 pN/µm from **Table S1**) we evaluated the forces generated by the cell as ~ 4 pN and ~ 30 pN, respectively.

Asymmetric values could arise from different adhesions of cells on the microspheres.

When adherent cells detach from their own substrates, they curl up and the cytoskeleton is less structured. In particular, the actin cortex of the cell remains, whereas the contracting actin stress fibers are only present in the adherent state. Through our setup we recreated cell adhesions, in a point-like manner, giving the cell the chance to reassemble actin structures. Resulting values of measured forces exceeded those needed to stall approximately eight (8) actin parallel-polymerizing filaments (1 pN)[42]. It has been proved that the average pulling force generated by a single myosin molecule interacting with a single actin filament is 3-4 pN[43]. Then, considering the direction of bead displacements and the force range measured, we were able to exclude that actin pushes against the trapped microspheres. Taken all together, these results suggested that the damping motion we collected for beads attached to a fibroblast might be the direct consequence of cell stiffening.

In an attempt to understand if such phenomenon is associated to the assembly of cellular actin structures, we performed the same experiment with fibroblasts after transfection treatment (see ESI). First, cell adhesion on point-like foothold (trapped microbeads) was confirmed by fluroscent modulus (**Figure S1**). Then, we investigated the cytoskeleton assembly in three instants of time, i.e. suspended cell without beads (t=0), 20 min after cell-bead attachment (t=20 min), and 30 min after stretching (t=50 min), using both DH and fluorescence moduli. We found that, at t=0 and t=20 min no actin organization was detected, as expected, confirmed by the DH-QPMs and fluorescence images reported in **Figure 4a-b,d-e**. Contrarily, in the time interval in which we recorded the displacement damping, i.e. after stretching (t=50 min), structured actin filaments were clearly visible (Fig.4c,f). In **Figure 4c** the QPM of the cell in false color at t=50 min reveals an enhancement of the OPD along the axis connecting the two microspheres, not present in the previous situations, indicating a modification of the internal cellular structure. In order to investigate such an arrangement, we recorded a fluorescence image at the same instant of time (**Figure 4f**). Surprisingly, we found evidence of a signal in correspondence of the actin filaments suggesting a cytoskeleton assembly inside the cell volume. In fact, the cytoskeleton modified its assembling over time and polarized the fluorescent filaments in the direction connecting the two external beads, as proved by the QPMs (**Figure 4c-f and S2**).

At this early stage, taking into account only the QPMs, it was not possible to confirm the presence of the cytoskeleton for two reasons: the low resolution and the lack of specificity in the OPD signal retrieved. However, it is difficult to imagine different causes that can produce such phase variation inside the cell in the particular setup we fabricated. Consequently, we believe that the enhancement found in the OPD, together with the cell stiffening and fluorescent observations were

ascribable to an attempt of early cytoskeleton assembling by the cell.

Conclusions

In summary, we developed a promising proof of concept/setup that gives cells, generally living in adhesion on 2D substrates, the possibility to adhere and mount their cytoskeleton in a 3D suspended configuration. In particular, our approach is able to detect the cytoskeleton and force generation in response to mechanical stimuli by nanomechanical characterization. The combined fluorescence imaging confirms cell stiffening by direct observation of the actin filaments-bundle, thus demonstrating the capability of our framework to investigate the material-cytoskeleton crosstalk in the early (a few hours) adhesion time and for different shape configurations. Moreover, the preliminary QPMs results are promising and permit to take into consideration DH as a label-free technique for cells nanomechanics investigation in the future.

Acknowledgments

References

1   S. Olof, J. Grieve, D. Phillips, H. Rosenkranz, M. Yallop, M. Miles, A. Patil, S. Mann and D. Carberry, Nano Lett., 2012, 12, 6018-6023.
2   S. Fusco, V. Panzetta, V. Embrione, P. A. Netti, Acta biomater., 2015, 23, 63-71.
3   D. A. Fletcher and R. D. Mullins, Nature, 2010, 463, 485-492.
4   A. R. Bausch and U. S. Schwarz, Nat. Mater., 2013, 12, 948-949.
5   E. Battista, F. Causa, V. Lettera, V. Panzetta, D. Guarnieri, S. Fusco, F. Gentile and P. A. Netti, Biomaterials, 2015, 45, 72-80.
6   B. Geiger, J. P. Spatz and A. D. Bershadsky, Nat. Rev. Mol. Cell Biol., 2009, 10, 21-33.
7   A. W. Orr, B. P. Helmke, B. R. Blackman and M. A. Schwartz, Dev. Cell, 2006, 10, 11-20.
8   W. R. Legant, C. K. Choi, J. S. Miller, L. Shao, L. Gao, E. Betzig and C. S. Chen, Proc. Natl. Acad. Sci. USA, 2013, 110, 881-886.
9   I. Schoen, W. Hu, E. Klotzsch and V. Vogel, Nano Lett., 2010, 10, 1823-1830.
10   S. Schlie, M. Gruene, H. Dittmar and B. N. Chichkov, Tissue Eng. Part C Method, 2012, 18, 688-696.
11   D. Stamenović and D. E. Ingber, Biomechanics and Modeling in Mechanobiology, 2002, 1, 95-108.
12   H. Zhang and K.-K. Liu, J. R. Soc. Interface, 2008, 5, 671-690.
13   K. Dholakia and T. Čižmár, Nat. Photon., 2011, 5, 335-342.
14   D. G. Grier, Nature, 2003, 424, 810-816.
15   D. J. Odde and M. J. Renn, Trends Biotechnol., 1999, 17, 385-389.
16   A. D. Franck, A. F. Powers, D. R. Gestaut, T. Gonen, T. N. Davis and C. L. Asbury, Nat. Cell Biol., 2007, 9, 832-837.
17   M. Gu, S. Kuriakose and X. Gan, Opt. Express, 2007, 15, 1369-1375.
18   N. Cardenas, L. Yu and S. K. Mohanty, 2011.
19   S. Raj, M. Marro, M. Wojdyla and D. Petrov, Biomed. Opt. Express, 2012, 3, 753-763.
20   S. Mohanty, K. Mohanty and P. Gupta, Opt. Express, 2005, 13, 4745-4751.
21   J. Guck, S. Schinkinger, B. Lincoln, F. Wottawah, S. Ebert, M. Romeyke, D. Lenz, H. M. Erickson, R. Ananthakrishnan and D. Mitchell, Biophys. J., 2005, 88, 3689-3698.
22   D. Mizuno, R. Bacabac, C. Tardin, D. Head and C. F. Schmidt, Phys. Rev. Lett., 2009, 102, 168102.
23   F. Schlosser, F. Rehfeldt and C. F. Schmidt, Phil. Trans. R. Soc. B, 2015, 370, 20140028.
24   Á. Barroso, M. Woerdemann, A. Vollmer, G. von Bally, B. Kemper and C. Denz, small, 2013, 9, 885-893.
25   S. A. Ermilov, D. R. Murdock, F. Qian, W. E. Brownell and B. Anvari, J. Biomech., 2007, 40, 476-480.
26   P. Jordan, J. Leach, M. Padgett, P. Blackburn, N. Isaacs, M. Goksör, D. Hanstorp, A. Wright, J. Girkin and J. Cooper, Lab. Chip, 2005, 5, 1224-1228.
27   L. Miccio, P. Memmolo, F. Merola, S. Fusco, V. Embrione, A. Paciello, M. Ventre, P. Netti and P. Ferraro, Lab. Chip, 2014, 14, 1129-1134.
28   M. DaneshPanah, S. Zwick, F. Schaal, M. Warber, B. Javidi and W. Osten, J. Display Technol., 2010, 6, 490-499.
29   P. Memmolo, L. Miccio, F. Merola, A. Paciello, V. Embrione, S. Fusco, P. Ferraro and P. Antonio Netti, Opt. Laser Eng., 2014, 52, 206-211.
30   K. Uhrig, R. Kurre, C. Schmitz, J. E. Curtis, T. Haraszti, A. E.-M. Clemen and J. P. Spatz, Lab. Chip, 2009, 9, 661-668.
31   M. Padgett and R. Di Leonardo, Lab. Chip, 2011, 11, 1196-1205.
32   G. Thalhammer, R. Steiger, M. Meinschad, M. Hill, S. Bernet and M. Ritsch-Marte, Biomed. Opt. Express, 2011, 2, 2859-2870.
33   A. Jesacher, C. Maurer, A. Schwaighofer, S. Bernet and M. Ritsch-Marte, Opt. Express, 2008, 16, 4479-4486.
34   G. R. Kirkham, E. Britchford, T. Upton, J. Ware, G. M. Gibson, Y. Devaud, M. Ehrbar, M. Padgett, S. Allen and L. D. Buttery, Sci. Rep., 2015, 5.
35   X. Yu, M. Cross, C. Liu, D. C. Clark, D. T. Haynie and M. K. Kim, J. Mod. Opt., 2012, 59, 1591-1598.
36   K. J. Chalut, A. E. Ekpenyong, W. L. Clegg, I. C. Melhuish and J. Guck, Integr. Biol., 2012, 4, 280-284.
37   B. Kemper, A. Vollmer, C. E. Rommel, J. Schnekenburger and G. von Bally, J. Biomed. Opt., 2011, 16, 026014-026014-026014.
38   A. S. Singh, A. Anand, R. A. Leitgeb and B. Javidi, Opt. Express, 2012, 20, 23617-23622.
39   P. Girshovitz and N. T. Shaked, Biomed. Opt. Express, 2012, 3, 1757-1773.
40   J. Reed, J. J. Troke, J. Schmit, S. Han, M. A. Teitell and J. K. Gimzewski, ACS nano, 2008, 2, 841-846.
41   G. Tomaiuolo, Biomicrofluidics, 2014, 8, 051501.
42   M. J. Footer, J. W. Kerssemakers, J. A. Theriot and M. Dogterom, Proc. Natl. Acad. Sci. USA, 2007, 104, 2181-2186.
43   D. Mehta and S. J. Gunst, J. Physiol., 1999, 519, 829-840.
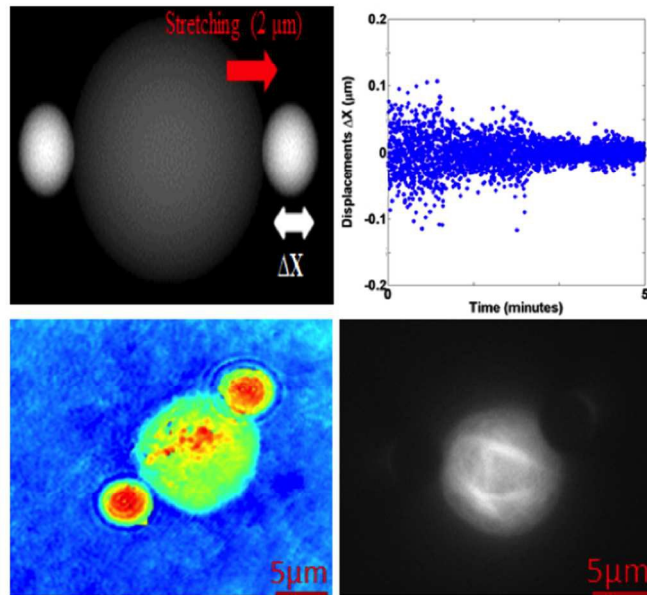
Cell suspended and stretched by two microbeads. The formation of inner cytoskeleton structures are reported by the dumped displacement, QPM phase change and fluorescent micrographs.

352x264mm (72 x 72 DPI)